Estimating error growth and shadow behavior

in nonlinear dynamical systems

D. Orrell

Institute for Systems Biology,

1441 N 34th Street, Seattle, USA

Phone (206) 732 1334, Email dorrell@systemsbiology.org

Abstract

In modeling nonlinear dynamical systems, error growth can arise both because of dynamical error in the model, and observational error in measurements of the underlying system. Errors thus introduced can be further amplified by the system dynamics. This paper develops a method to approximate error growth, based on the model drift, for the general case when the model is given by a (possibly large) set of ordinary differential equations. The ability of the model to shadow (stay close to) the true system is analyzed, and a criterion for model quality based on the error dynamics is proposed. Examples are given with a range of models, which are chosen to be representative of different types of model error.

1 Introduction

Nonlinear dynamical models are frequently used to approximate and predict observed physical systems. Such models will be subject to errors both in the model dynamics, and the observations of the underlying 'true' system. Dynamical errors may be the result of parameterised, unmodeled, or stochastic processes in the true system, or other shortcomings in the model equations. Observational errors can be caused either by errors in measurement of the variables, or because what is being measured differs from the idealised model variables. Either type of error will be acted on by the nonlinear dynamics; this is particularly a concern if the model is strongly chaotic, since small errors may be magnified due to sensitivity to initial condition.

In high dimension models, of the sort used in problems such as weather prediction or increasingly the biological sciences, it can be hard to develop an intuitive understanding of model accuracy or error growth (Keller, 2002). Perhaps the ultimate example of complicated nonlinear models are those used in biological oceanography (Robinson et al., 1999), which combine geophysical forecasts with biological models. As models grow in complexity, so tools are required to test and improve their accuracy.

Two types of questions typically arise when testing a model. The first is how

well one model agrees with another. This will apply when different models are compared in inter-model experiments, or the effect of a change in parameters is assessed as in robustness tests (Morohashi et al., 2002). Such experiments take place on the computer, so all the relevant equations are known. There is therefore no observational error, though there may be an equivalent type of error in translating from the variables of one model to another.

The second type of question relates to the comparison of models with real data. For such observed systems the equations are not known (otherwise the best model would be known), or do not exist. One then wishes to know whether the model is consistent with the data, and has the appropriate dynamics. Perhaps the most fundamental, and desirable, quality of a model is that it be able to accurately predict the evolution of the system.

To address either type of question, a measure of model quality is required; in inter-model experiments, to see whether the models are in some sense converging, and in experiments with real data, to fit the model parameters, or determine how well the model approximates the observations. We need to be able to estimate error magnitude, and determine whether it is primarily due to observational error, dynamical error, or the effects of chaos. If the cause is the model dynamics, then error analysis can not only lead to an improved model, but may point towards an

unexpected feature of the system not present in the model.

A number of techniques have been used in the literature to compare and validate models. Some are based on properties of the model and system attractors, such as dimension, entropy, Lyapunov estimates, or topology (Small and Judd, 1998; Schreiber and Kantz, 1996; Letellier et al., 1995); or comparing model and system bifurcation diagrams as a parameter is changed (Aguirre and Billings, 1994). While these methods provide useful insight into properties of the model attractor, our concern here is less with long-range statistics than short-term prediction, although in some cases the two can be linked (Orrell, 2003). Other approaches for validating models include those based on noise reduction techniques (Kostelich and Yorke, 1990), or likelihood methods (Ozaki et al., 2000; Heald and Stark, 2000).

The approach of this paper differs in that it is based on an analysis of error dynamics. Given a particular model, the aim is not so much to validate it or optimize it, but rather to examine the various causes of error growth, and then develop a formula which approximates the error using quantities that are easily testable even in high-dimensional models. This approach then leads naturally to a particular measure of model quality based on the drift which was presented in a previous work (Orrell, 2005). The methods apply in the general case when

the model is given by a set of ordinary differential equations (ODE's), and apply whether this is derived from first principles, or is obtained by fitting the observed data (see for example Brown et al., 1994).

Section 2 begins by examining the basic dynamics of error growth, considering both dynamical and observational errors. Section 3 provides examples of error growth using a variety of model/system pairs, and Section 4 develops an error growth formula for the case when both dynamical and observational errors are stochastic. Section 5 argues that the ability of a model to shadow (stay close to) the true system is largely a function of the expected forecast error. Finally, Section 6 discusses how the results lead to a measure of model quality. The emphasis is on predictability in the near to medium-range, which for the chaotic systems translates to about 3 or 4 times the internal doubling time.

Results are illustrated using chaotic versions of the Lorenz '63 and '96 systems, which are typically used as toy systems in the atmospheric sciences or geophysics; the Chua circuit; a non-chaotic version of the Vance-Gilpin system, which is a predator-prey model; and a weather model. The details of the models and systems are provided in the Appendix, and were chosen in order to illustrate various types of model error and system behaviour.

6

2   Dynamics of error growth

Suppose we have a model

$$\frac{d\mathbf{s}}{dt} = \mathbf{G}(\mathbf{s}(t)) \tag{1}$$

of some process, and wish to compare the model predictions with observations $\mathbf{y}(t_j)$ of the underlying system. In a physical system, the observations are not usually expressed in the same variables as the model, so we implicitly assume that the observations have been mapped into the model parameters. For simplicity, we also assume that the observations occur at equally spaced intervals $t_j = j\Delta t$.

As illustrated in panel A of Figure 1, we define $\mathbf{s}_j(t)$ for $t \geq t_j$ to be the model trajectory initiated at time t_j on the point $\mathbf{y}(t_j)$. The drift vector is defined as

$$\mathbf{d}(t_K) = \sum_{j=0}^{K-1} \mathbf{f_j}, \tag{2}$$

where $\mathbf{f_j} = \mathbf{s}_j(t_{j+1}) - \mathbf{y}(t_{j+1})$ are a series of short forecast errors. The propagated drift is defined as

$$\mathbf{d_p}^m(t_K) = \sum_{j=0}^{K-1} \mathbf{M}(t_K, t_{j+1})\mathbf{f_j}, \tag{3}$$

where

$$\mathbf{M}(t_K, t_j) = e^{\int_{t_j}^{t_K} \mathbf{J}((\mathbf{y}(t))dt} \tag{4}$$

7

is the model linear propagator (Strang, 1986) and $\mathbf{J}((\mathbf{y}(t))$ is the Jacobian of the model ODE. Since $\mathbf{y}(t)$ is only known at times t_j, the linear propagator must be evaluated in a discrete fashion. The calculations are shown schematically in Figure 2; the drift is a sum of forecast errors, while in the propagated drift each short forecast error is magnified by an amount corresponding to the linear propagator.

We claim that the propagated drift can be used to approximate error growth over the short to medium term. To see this, let $\mathbf{x}(t)$ be a piecewise linear interpolation of the observations, so $\mathbf{x}(t_j) = \mathbf{y}(t_j)$ for all j, and is linear between these points. Such a curve is illustrated by the solid line in panel A of Figure 1. Setting $\mathbf{r}(t) = \mathbf{s}(t) - \mathbf{x}(t)$, it follows that

$$
\begin{aligned}
\frac{d\mathbf{r}(t)}{dt} &= \frac{d\mathbf{s}(t)}{dt} - \frac{d\mathbf{x}(t)}{dt} \\
&= \mathbf{G}(\mathbf{x}(t) + \mathbf{r}(t)) - \mathbf{G}(\mathbf{x}(t)) - \epsilon^m(t) \\
&\approx \mathbf{J}(\mathbf{x}(t))\mathbf{r}(t) - \epsilon^m(t)
\end{aligned}
\tag{5}
$$

where

$$
\epsilon^m(t) = \frac{d\mathbf{x}(t)}{dt} - \mathbf{G}(\mathbf{x}(t)),
\tag{6}
$$

which is defined almost everywhere (i.e. except at times t_j). As can be seen by

8

direct substitution, a solution to this approximate growth equation is

$$\mathbf{r}(t_K) \approx - \int_0^{t_K} \mathbf{M}(t_K, t) \epsilon^m(t) dt. \tag{7}$$

Since $\mathbf{f_j} \approx -\epsilon^m(t_j)\Delta t$, the propagated drift is a discrete form of this equation.

The length of time for which the approximation is valid will depend on a number of factors. Eq. 5 represents a linearization of the dynamics around the orbit $\mathbf{x}(t)$, which for a nonlinear system will break down as errors $\mathbf{r}(t)$ become larger. It will therefore be more accurate for shadow orbits, discussed in Section 5, which have smaller errors by definition; or for systems with a stable attractor, where the errors do not necessarily grow with time, as discussed at the end of Section 4. Another source of error is the discretization represented by the timestep Δt; this can be checked for example by using a smaller (or larger) timestep to see if the results are converging. The best way to get a feeling for the method's accuracy for a particular model/system pair is to compare the estimates with actual errors, as is done below for a number of examples.

In the above argument, we have not specified whether errors are due to observational errors, or dynamical errors, or a combination of the two. If a system is known only through observations which contain unknown error, then it is not pos-

sible to isolate the error components without making extra assumptions (Smith, 2000; Judd and Smith, 2001). For example, in panel A of Figure 1 the system trajectory $\mathbf{x}(t)$ is an interpolation of the observations, so observational error is zero by definition and all errors appear as dynamical terms; but another choice of $\mathbf{x}(t)$, as in panel B of Figure 1, which does not exactly interpolate the observations, will include an observational error component.

Suppose then that we hypothesize that the observations $\mathbf{y}(t_j)$ are obtained from the 'true' system trajectory $\mathbf{x}(t)$, where $\mathbf{x}(t)$ is a differentiable curve expressed in model variables. Setting

$$\epsilon^m(t) = \frac{d\mathbf{x}(t)}{dt} - \mathbf{G}(\mathbf{x}(t)) \tag{8}$$

we can then write

$$
\begin{aligned}
\frac{d\mathbf{x}(t)}{dt} &= \mathbf{G}(\mathbf{x}(t)) + \epsilon^m(t) \\
\mathbf{y}(t_j) &= \mathbf{x}(t_j) + \epsilon^o(t_j).
\end{aligned}
\tag{9}
$$

Relative to the trajectory $\mathbf{x}(t)$, the model is therefore subject to dynamical errors given by $\epsilon^m(t)$ and observational errors $\epsilon^o(t)$. We can then ask what forecast errors would result from this combination of observational and dynamical error.

10

Note that Eq. 9 does not imply the equations of the system are assumed to be the same, even in structure, as those of the model Eq. 1; the term $\epsilon^m(t)$ represents the difference between the two as measured on the particular trajectory $\mathbf{x}(t)$. Indeed, the system may be a function of variables other than the model variables, as seen in the next section; or may not be computed from an ODE at all. For example, in weather forecasting, errors are typically measured relative to a smoothed version of the observations known as the analysis. The system trajectory $\mathbf{x}(t)$ is therefore given by the analysis at each time t, rather than the integration of an ODE. The error term $\epsilon^m(t) = \frac{d\mathbf{x}(t)}{dt} - \mathbf{G}(\mathbf{x}(t))$ in this case is a highly complicated function of time. The reason for writing the system in the form of Eq. 9 is because we typically are interested in determining, and if possible reducing, the magnitude of the error term $\epsilon^m(t)$.

Using the approximations

$$\mathbf{s}(t_{j+1}) \approx \mathbf{y}(t_j) + \Delta t \mathbf{G}(\mathbf{y}(t_j)) \tag{10}$$

$$\mathbf{x}(t_{j+1}) \approx \mathbf{x}(t_j) + \Delta t \mathbf{G}(\mathbf{x}(t_j)) + \Delta t \epsilon^m(t_j) \tag{11}$$

$$\mathbf{G}(\mathbf{x}(t_j) + \epsilon^o(t_j)) \approx \mathbf{G}(\mathbf{x}(t_j)) + \mathbf{J}(\mathbf{x}(t_j)\epsilon^o(t_j) \tag{12}$$

11

the drift is seen to satisfy

$$\mathbf{d}(t_K) \approx \mathbf{d}^m(t_K) + \mathbf{d}^o(t_K), \tag{13}$$

where

$$\mathbf{d}^m(t_K) = -\Delta t \sum_{j=0}^{K-1} \epsilon^m(t_j) \tag{14}$$

is the drift due to the dynamical errors, and

$$\mathbf{d}^o(t_K) = \Delta t \sum_{j=0}^{K-1} \mathbf{J}(\mathbf{x}(t_j))\epsilon^o(t_j) + \epsilon^o(t_0) - \epsilon^o(t_K) \tag{15}$$

is the drift due to the observational error (Orrell, 2005).

Referring to Figure 1, if $\mathbf{x}(t)$ equals the curve in panel A, then observational error is zero and all error is dynamical; but if $\mathbf{x}(t)$ is the curve in panel B, then part of the error is observational. In either case the total drift, Eq. 2, is the same, and the drift does not distinguish between them. However if the observational error is assumed to be Gaussian noise, then Eq. 15 can be used to estimate the error components as discussed in (Orrell, 2005). Our aim here is to show how the propagated drift can be used to estimate forecast error, for an assumed amount of observational and dynamical error. In the next section we illustrate its use for

12

a number of examples, before going on to develop approximations that can be applied even to high-dimension models.

3   Examples of error growth

Dynamical errors can be the result, among other things, of error in the values of the parameters, errors due to parameterization of complex processes, and errors due to stochastic effects. Figure 3 shows error growth for three different model/system pairs, chosen to represent these basic types. In the upper panels, the system is the standard Lorenz '63 system, but the model has the Reynold's parameter set to $R = 28.28$. Referring to Eqs. A1, the difference between the equations of the true system and the model occurs only in the equation for y, where it introduces a dynamical error of $0.28x$ (see also (Chu, 1999)). The error is therefore highly correlated over time periods for which x varies only slightly. This model/system pair is representative of situations where model error arises due to parameter error.

The second system in the middle panels is the two-level Lorenz '96 system, given by Eqs. A3, which involves two sets of variables (Lorenz, 1996). The 40D version involves 8 $\tilde{x}$ variables, which are relatively large-scale and slow-varying, and 32 $\tilde{y}$ variables which are small-scale and fast-varying, and can be viewed as

sub-gridscale processes. The large-scale $\tilde{x}$ variables can therefore be modeled with the *constant model* (so-named because of the constant forcing), which is the regular Lorenz '96 model with forcing $F = 9.62$ chosen to minimise the expected RMS dynamical error. This model/system pair is therefore representative of situations where model error is due to the parameterization, in this case by a constant, of a complex process. The dynamical error term $\epsilon^m(t)$ in Eq. 9 has a complicated dependence on the $\tilde{y}$ variables, which in turn are a function of the $\tilde{x}$ variables.

The lower panels show errors for the Chua circuit (Madan, 1993; Matsumoto et al., 1985), where the model is given by Eqs. A5, but the system has additional stochastic dynamical terms of magnitude $\Delta F = 1$, updated each $\Delta t = 0.01$ time units. It is representative of situations where model error arises due to unparam-eterized effects which are uncorrelated in time and can be viewed as essentially stochastic. This type of error is discussed in more detail in the next section.

The left panels of Figure 3 show the drift $d^m(t)$ in the absence of observational error, while the right panels include the effect of Gaussian observational error of magnitude $S = 0.1$. From Eqs. 13 and 15,

$$\mathbf{d}(t_K) \approx \mathbf{d}^m(t_K) + \Delta t \sum_{j=0}^{K-1} \mathbf{J}(\mathbf{x}(t_j))\epsilon^o(t_j) + \epsilon^o(t_0) - \epsilon^o(t_K). \qquad (16)$$

14

Therefore the effect of the added noise is to increase the drift so that

$$d(t_K)^2 \approx d^m(t_K)^2 + S^2\beta^2 t_K \Delta t + 2S^2, \qquad (17)$$

where β is the standard deviation of $\frac{1}{S}\mathbf{J}(\mathbf{y}(t_j))\epsilon^o(t)$ as evaluated over a large sample of points (Orrell, 2005). The term $2S^2$ is caused by the initial and final observational errors. The term involving β is due to the effect of the observational error on each small forecast error, and is often small enough to be ignored, in which case

$$d(t)^2 \approx d^m(t)^2 + 2S^2. \qquad (18)$$

Error growth can in either case be approximated by the propagated drift, Eq. 3. The calculation can be simplified by noting that the linear propagator over the time $t_j = j\Delta t$ to t_K can be written as a product of the linear propagators over each intermediate time step. As shown by the solid line, the propagated drift is a good match for the errors over the times shown.

The accuracy of the propagated drift will vary from point to point, and it is clearly easier to match the root-mean-square error than the exact error at each point. For example, in the case of the Lorenz '63 model with a one percent error in R, the difference between the approximated and actual errors is seen to be greatest

15

near the tips of the attractor, where both the model error and the acceleration of the system variables are greatest.

4 Stochastic errors

While it is possible to calculate the linear propagator explicitly for low or medium-dimensional models, this may not be the case when the number of dimensions becomes very high. An example is weather models, which can contain of the order 10^7 variables. Even with smaller models, it may be desirable to obtain a rapid estimate of error magnitude without explicitly calculating the linear propagator. In this section, we show how RMS error growth can be approximated in such situations if it is assumed that the errors are essentially stochastic.

Suppose that the dynamical error $\epsilon^m(t_j)$ is a vector whose components are Gaussian random variables, with mean zero and a magnitude of standard deviation ΔF, updated every Δt time units as in a Wiener process (Wiener, 1923). Referring to Eq. 2, the total RMS drift $d^m(t_K)$ due to dynamical error has

$$d^m(t_K)^2 = \sum_{j=0}^{K-1} \Delta F^2 \Delta t^2 = \Delta F^2 t_K \Delta t \qquad (19)$$

16

so

$$d^m(t_K) = \Delta F \sqrt{\Delta t} \sqrt{t_K}, \tag{20}$$

which grows in a square-root fashion like a random walk.

From Eq. 3, the propagated drift is

$$\mathbf{d_p}^m(t_K) = - \sum_{j=0}^{K-1} \mathbf{M}(t_K, t_{j+1}) \epsilon^m(t_j) \Delta t. \tag{21}$$

Suppose that small perturbations $\mathbf{e}_0$, of RMS magnitude e_0, made to the model initial condition, grow under the model dynamics to an expected RMS magnitude of $\mathbf{e}(t)$; and let

$$p(t) = \lim_{e_0 \to 0} \frac{e(t)}{e_0}. \tag{22}$$

The function $p(t)$ then accounts for the RMS growth of a small initial perturbation under the action of the linear propagator. It can be calculated by making an ensemble of small perturbations to the model trajectory, at an ensemble of initial conditions, and determining the RMS error growth. Then the RMS magnitude of the propagated drift satisfies

$$d_p^m(t_K)^2 \approx \sum_{j=0}^{K-1} p(t_K - t_{j+1})^2 \Delta F^2 \Delta t^2. \tag{23}$$

17

Calculating the sum in an iterative manner gives

$$d_p^m(t_0)^2 = 0$$

$$d_p^m(t_j)^2 = d_p^m(t_{j-1})^2 + p(t_{j-1})^2 \Delta F^2 \Delta t^2. \qquad (24)$$

This approach to estimating error growth is demonstrated in Fig. 4 for the Vance-Gilpin model (Vance, 1978; Gilpin, 1979), Eqs. A7 in the Appendix. For the parameters as given in the Appendix, the model has a stable limit cycle shown in the top left panel by the solid line, with a period of about 30 time units. The top right panel shows root-mean-square (RMS) errors due to an initial error of magnitude 0.1. Perturbations grow rapidly for the first ten time units, then begin to oscillate. The perturbed orbit is drawn back onto the limit cycle, but is out of phase with the unperturbed orbit. The estimate of forecast error in the lower panels, from Eq. 23, agrees well with the actual errors.

For many models, it is possible to develop a simple formula for the total error growth due to the propagated drift by using an estimate for the error propagation function $p(t)$. As an example, the right panel of Figure 5 shows RMS errors due to an initial error of magnitude 0.5 for two chaotic systems. The first is the Lorenz '63 system (Lorenz, 1963), given by Eqs. A1 in the Appendix, with Reynold's

number $R = 28$. The second system is the 8D Lorenz '96 system, given by Eqs. A2 (Lorenz, 1996; Orrell and Smith, 2003). The forcing was set to $F = 13.2$ so that the doubling time was comparable to that of the Lorenz '63 system; however the two systems differ in both dimension and the nature of the equations. Typical time series plots of x and x_1 are shown for the Lorenz '63 and '96 systems respectively in the left panels.

A possible choice for $p(t)$ in this case might be an exponential growth function, based on the leading Lyapunov exponent. However, while errors in a chaotic system typically grow for intermediate time scales in an exponential-on-average fashion (Smith et al., 1999) the error growth here actually has three phases: an initial phase of nearly flat growth, a quasi-exponential growth phase, and (at higher times) a final saturation phase. One way to approximate this is to assume that the initial condition error creates a displacement which grows exponentially, but in a direction orthogonal to the initial error. The error propagation function $p(t)$ is then approximately given by

$$p(t) \approx \sqrt{1 + (e^{at} - 1)^2}. \qquad (25)$$

The doubling time in the exponential phase is $t_d = log(2)/a$. This estimate with

$t_d = 0.17$ ($a = 4.1$) is shown by the solid line in Figure 5. The fit is good until about $t = 0.3$, and loses all accuracy at about $t = 0.7$, so about 4 times the doubling time.

Given this approximation for $p(t)$, one can estimate the RMS magnitude $d_p^m(t_K)$ of the propagated drift $\mathbf{d_p}^m(t_K)$ due to the model by summing the terms in Eq. 23. The result is

$$d_p^m(t_K)^2 \approx \Delta F^2 \Delta t^2 \left(\sum_{j=0}^{K-1} 1 + (e^{a(K-j-1)\Delta t} - 1)^2 \right) \quad (26)$$

$$= d^m(t_K)^2 + \Delta F^2 \Delta t^2 q(t_K)^2 \quad (27)$$

where

$$q(t_K)^2 = \left(\frac{e^{at_K} - 1}{e^{a\Delta t} - 1} \left(\frac{e^{at_K} + 1}{e^{a\Delta t} + 1} - 2 \right) + \frac{t_K}{\Delta t} \right). \quad (28)$$

The first term in Eq. 27 is the dynamical drift, while the second term, shown schematically in the middle panel of Figure 2 by the dotted line, accounts for the quasi-exponential magnification of dynamical errors by the error propagation function.

Suppose now that the target trajectory contains Gaussian observational noise, uncorrelated over the time step Δt, with expected RMS magnitude S. The propa-

20

gated drift can then be determined in the same way as above, to give

$$d_p(t_K)^2 \approx d^m(t_K)^2 + (\Delta F^2 + S^2\beta^2)\Delta t^2 q(t_K)^2 + S^2 p(t_K)^2 + S^2 \qquad (29)$$

where β is as in Eq. 17. The first two terms in the above equation account for the growth of the short forecast errors in the drift calculation. The last two terms represent the growth of the initial and final observational errors which appear in Eq. 15.

Figure 6 compares actual and estimated error growth for the Lorenz '63 and Lorenz '96 systems for a range of dynamical and observational noise. The parameter β was calculated as 11.5 in (Orrell, 2005) and makes only a small contribution to the total error. The error estimates match actual results reasonably well, whether the error is primarily due to observations (low ΔF, high S) or the dynamics (high ΔF, low S). It is interesting to note that, for these and other systems, error growth is often almost linear over a large range, as the negative curvature of the drift is balanced by the positive curvature of the exponential terms: linear error growth does not imply a linear error mechanism.

This is seen also in Figure 7, which shows RMS errors for a weather model over a 15 day period in December 2000 (circle symbols). The model is the opera-

21

tional model used by the European Centre for Medium-Range Weather Forecasts (ECMWF), and errors are measured relative to the analysis in the total energy metric, which accounts for wind and temperature errors at all model levels. Details of the model and experiment are given in (Orrell et al., 2001). As shown in that paper, the short forecast errors have low correlation from time to time, and the drift grows in an approximately square-root fashion, so we can approximately model the errors as being stochastic model errors, with magnitude equal to the 12 hour error. The analysis is obtained by the 4DVAR technique (Cohn, 1997) which adjusts the observations to better fit model predictions. As discussed in (Orrell, 2005), this has the effect of reducing the apparent observational errors (which in any case have a relatively small effect on the drift). The doubling time of small perturbations in this metric is about $t_d = 3$ days (Orrell, 2002). Using the fit Eq. 29 with this doubling time, and a ΔF which matches the initial error, gives the curve shown by the solid line in Figure 7. The effect of the term involving β was ignored due to the model's relatively low sensitivity to initial condition. While it is dangerous to read too much into such graphs - model error is best measured by methods such as the drift, and doubling time by measuring the growth of small perturbations - we can at least say that the observed growth of forecast errors is consistent with previous estimates of these quantities.

A formula for error growth is useful in that it shows how observational and dynamical errors convolute; can be used to compare estimates of these terms, obtained from measurements of the drift and the error propagation function, with the total observed error; and can be applied even to large models such as weather models. It can also be used to obtain rough confidence bands around forecasts. For example, suppose that we wish to estimate the standard deviation of an otherwise stable system when stochastic forcing terms ΔF are added; and that the error propagation function for a model can be adequately approximated by the first-order decay function

$$p(t) \approx e^{-t/t_e}, \tag{30}$$

where t_e is an exponential decay time. Then from Eq. 23, the propagated drift of the stochastic orbit relative to the stable point is

$$d_p^m(t_K)^2 = \sum_{j=0}^{K-1} p(t_K - t_{j+1})^2 \Delta F^2 \Delta t^2 \tag{31}$$

$$= \Delta F^2 \Delta t^2 \sum_{j=0}^{K-1} e^{2\frac{t_K - t_{j+1}}{t_e}} \tag{32}$$

$$\approx \Delta F^2 \Delta t \frac{t_e}{2} \left(1 - e^{\frac{-2t_K}{t_e}}\right), \tag{33}$$

which asymptotes at large t_K to a variance of $\Delta F^2 \Delta t \frac{t_e}{2}$. The magnitude of fluc-

tuations can therefore be estimated from a knowledge of the stochastic terms and the decay dynamics, and can be interpreted as a dynamical balance between the former, which tend to push the system away from the attractor, and the latter, which draw it back. This technique has been used to estimate fluctuations in biological systems at a cellular level (Orrell and Bolouri, 2004), which occur due to the inherently stochastic nature of the reactions (Gillespie, 1976). Since an ODE simulation of the system initiated at the steady-state will be constant, the standard deviation can be used to produce a confidence band around the ODE solution.

5 Shadowing

The preceding sections have explored how forecast errors arise when the model is initiated on the observation of the true system. Since both the model and the observations are assumed to have errors, it is interesting to ask whether it is possible to find some nearby initial condition for which the model trajectory stays close to, or shadows, the observed system (Smith, 1996; Gilmour, 1998).

The ability to shadow presents a fundamental test of the simplifications and assumptions that underly most models. For example, if a model can shadow, then a picture of the likely future behavior of the true system can be determined by

running a large number of model forecasts from perturbed initial conditions; while if the model is incapable of shadowing, no such ensemble of forecasts will contain a member that stays close to the true trajectory (Orrell, 2005a). Assimilation schemes such as 4DVAR or ensemble-based techniques (Gronnevik and Evensen, 2001; Hansen, 2002) will also be affected. Shadowing in nonlinear dynamical models is complicated by the effects of chaos and sensitivity to initial condition. The latter seems a double-edged sword; if a model is highly sensitive to initial condition, then forecast errors will grow rapidly, which makes the task of reducing the error harder. On the other hand, a small change in initial condition produces a larger change downstream.

Given a shadow time τ and radius r, the shadowing problem consists of seeking a model orbit $\mathbf{s}(t)$ for which the error vector

$$\mathbf{e}(t) = \mathbf{s}(t) - \tilde{\mathbf{s}}(t) \tag{34}$$

satisfies $\|\mathbf{e}(t)\| \leq r$ for $0 \leq t \leq \tau$. [1] Model orbits which shadow a trajectory of

[1]Note that this definition is distinct from the problem addressed in the *Anosov-Bowen shadowing lemma* (Anosov, 1967; Bowen, 1975) which states conditions under which a true trajectory can be found which shadows a numerical model trajectory. Our aim is the opposite: we wish to determine whether model trajectories shadow the true orbit. Under this definition, there is no question of whether a model *can* shadow a target orbit, only within which radius; any model will shadow for time τ if the shadow radius is set to the maximum error over the time period 0 to τ.

the true system can be found by optimization methods which choose the optimal initial condition. An example of a shadow orbit is shown in Figure 8 for the Lorenz '63 system with shadow radius $r = 0.3$. Such optimization methods can become expensive in large systems, where the search must be carried out in a high-dimensional space. In this section, however, we argue that error behaves in a see-saw fashion: choosing the correct initial condition will reduce the forecast error, but only (in an average sense) by a certain amount, which is roughly equal to, or even smaller than, the original displacement. To reduce the expected final error, one must introduce large initial displacements - even if the model is sensitive to initial condition. Thus shadowing behaviour is largely a function of forecast error, especially when model error is significant.

The result is derived by noting that an approximate equation for the error growth with a small initial displacement $\mathbf{e}(0)$ is given by

$$\mathbf{e}(\tau) \approx \mathbf{M}(\tau, 0)\mathbf{e}(0) + \mathbf{d_p}(\tau).\tag{35}$$

A ball of initial conditions with initial displacement r is therefore distorted into an ellipse by the linear propagator (Golub and Loan, 1989), and displaced by the propagated drift. Following the argument in (Orrell et al., 2001), and using the

26

propagated drift rather than the drift as an estimate for forecast error, then so long as the model is dissipative and contracts volumes in phase space (Ott, 1993), the expected shadow radius r within which the model can shadow for time τ satisfies

$$\sqrt{\langle r^2 \rangle} \geq \frac{\|\mathbf{d_p}\|}{2}. \tag{36}$$

This relationship between shadow times and forecast error can break down for at least two reasons. The first is that forecast times are such that the linear propagator does not accurately capture the dynamics of shadow orbits. This can occur for example at long forecast times. The second reason is correlations between the propagated drift and the singular vectors of $\mathbf{M}(\tau, 0)$. In general, this is less likely to occur if the propagated drift is dominated mostly by model error, which is assumed to be uncorrelated with the singular vectors. As a rough guide, the theory should hold for times greater than the time t_1 at which forecast error is dominated by the drift; but less than the time t_2 at which the propagated drift ceases to be accurate.

We here illustrate the shadowing process for three of the model/system pairs; Lorenz '63 with a one percent error in R; the Lorenz '96 two-level system approximated by the constant model; and the Chua circuit with stochastic dynam-

ical terms. For a particular shadow radius r, an optimization program based on the simplex method (Press et al., 1986) was used to find a model initial condition such that the model trajectory stayed within r of a true trajectory for the maximum time. Statistics were obtained by performing the experiment for 50 different initial conditions of the true system. The entire process was then repeated at different values of the shadow radius r.

Figure 9 compares a plot of median forecast error as a function of time, with a reflected plot of median shadow time as a function of shadow diameter $2r$, for the two systems. The left panels show the case without observational errors, while in the right panels Gaussian errors of standard deviation $S = 0.1$ were added to the observations of the system. Plots using root-mean-square statistics give similar results in most cases, but the Lorenz '63 shadow results are highly skewed towards short shadow times, with the occasional very long shadow orbit, so the median is more representative of shadow behaviour.

For either system, the forecast error is close to the shadow diameter for shorter times. The effect of noise is to increase both forecast error and shadow diameter, but the latter by a larger amount than the former. This reflects the fact that it is harder to shadow a noisy orbit than a smooth one.

The forecast error thus provides a useful guide to expected shadow behaviour.

28

Of course, the best way to estimate shadow times is to search directly for shadow orbits. However, not only can this be expensive, but one may also lack confidence in the results if the optimization technique fails or there are concerns about multiple minima. Comparing the results from shadow experiments with those predicted from the forecast error provides a good 'sanity check' on the results. If the two methods differ significantly, then it should be possible to determine the reason by closer analysis of the error dynamics.

A model's ability to shadow is of key importance to many areas of physical, biological, or economic forecasting. If a model can not shadow within a reasonable radius, then even an ensemble of forecasts from perturbed initial conditions will not stay close to the true system. The results here imply that shadowing is a question of give and take; one can reduce the expected final error, but only by giving up a large initial displacement. This holds even if the model is sensitive to initial condition, provided that model error is significant. The main determinant of both shadowing and overall model quality is therefore simply the expected forecast error.

6 Conclusions

In this paper we have shown that error growth, even in high-dimensional models, can be analyzed by use of the error propagation function, defined in Eq. 22, and the drift, Eq. 2. The former is a measure of sensitivity to initial condition, while the latter is a measure of model error and observation error. The two effects are combined in the propagated drift, Eq. 3. For many models, the error propagation function can be modeled and a formula for total error growth derived. For models which do not show simple error growth patterns, it is still possible to estimate error by explicitly calculating the error propagation function. The error dynamics affect not only the expected forecast error, but also as shown by Eq. 36 the model's ability to shadow the true system. While the techniques have been demonstrated for only a few systems, they are based in the dynamics of error growth, so hold quite generally and can be applied with suitable caution to a range of model/system pairs.

The results can be used in a number of ways. Both the drift and the error propagation functions can be determined from simple experiments. The formula for error growth then gives an estimate of expected forecast error, which can be compared with, or used to predict, the observed error. Since shadow behaviour is related to forecast error, one can also estimate the radius within which the model

30

is expected to shadow. This information can be used to determine the perturbation radius for ensemble schemes, or assess the effect of model error on variational data assimilation techniques. The techniques can be applied even for high-dimensional models of observed physical systems such as the atmosphere.

Perhaps the main application of these methods is to develop criteria for model quality. The magnitude of error at a particular time will depend on a number of factors such as the extent of observation error, the model's sensitivity to initial condition, and the dynamical error. In many modeling situations, however, only the latter is within the modeler's direct control; so total forecast error is best reduced by a decrease in dynamical error. For example, a small improvement in parameterization may have a minimal effect on the model's sensitivity to initial condition, but reduce model error quite significantly (Orrell, 2003). A simple criterion for model quality is therefore that it should have the minimum dynamical error. Since the expected one-step forecast error for stochastic errors is

$$e(\Delta t) \approx \sqrt{2S^2 + (F\Delta t)^2}, \tag{37}$$

and S is assumed to be a constant, this requirement translates to saying that the model should minimise the expected one-step forecast error, as in conditional

least-squares (Klimko and Nelson, 1978; Dennis et al., 1995; Tong, 1990). In practice, however, it is often easier and more effective to minimize the drift, since it has the effect of amplifying the dynamical error relative to the observational error (Orrell, 2005). Because of the relationship between drift, forecast error and shadow behaviour, a model which minimises the drift also has optimal shadow performance.

We assume of course that observations are sufficiently frequent, however there is no need for the time step Δt to approach zero. The main requirement is that error growth over one time step should be be primarily due to the combined effects of the dynamical and observational noise, rather than the nonlinear dynamics, so that the discretization in Eq. 3 is accurate. This will certainly be the case for most inter-model experiments, but also for many physical situations as well.

In one sense, this result is rather trivial and obvious; clearly one wishes to reduce the one-step forecast error and therefore the drift. In another sense, however, it might be quite surprising, for it implies that the short term forecast errors which make up the drift are not necessarily a transient 'spin-up' phenomenon, but the major determinant of predictability. It also provides a framework for questions about model optimization and comparison. For example, given a particular model structure, which is the best choice of parameters? Or given a selection of

different models, which gives the optimal performance? Is a hierarchy of progressively more refined models converging to a single solution, or does a small change give radically different results? Techniques such as calculating the model drift or computing shadow orbits are simple to implement and should provide a useful approach to answering these questions.

Appendix

The equations for the Lorenz '63 system are:

$$
\begin{aligned}
\frac{dx}{dt} &= -\sigma x + \sigma y \\
\frac{dy}{dt} &= -xz + Rx - y \\
\frac{dz}{dt} &= xy - Bz
\end{aligned}
\tag{A1}
$$

where the parameters are set to $\sigma = 10$ and $B = 8/3$. The classic value of the Reynold's number is $R = 28$, for which the system is chaotic.

The equations for the Lorenz '96 system are

$$
\frac{dx_i}{dt} = x_{i-1}(x_{i+1} - x_{i-2}) - x_i + F,
\tag{A2}
$$

where the index $i = 1$ to 8 is cyclic, so $x_{i+8} = x_i$. For forcing $F = 13.2$, the system is chaotic and has approximately the same sensitivity to initial condition as the Lorenz '63 system.

The two-level system is a higher-dimension version of the Lorenz '96 system

with equations:

$$\frac{d\tilde{x}_i}{dt} = \tilde{x}_{i-1}(\tilde{x}_{i+1} - \tilde{x}_{i-2}) - \tilde{x}_i + \tilde{F} - \frac{hc}{b}\sum_{j=1}^{m}\tilde{y}_{i,j}$$

$$\frac{d\tilde{y}_{i,j}}{dt} = cb\tilde{y}_{i,j+1}(\tilde{y}_{i,j-1} - \tilde{y}_{i,j+2}) - c\tilde{y}_{i,j} + \frac{hc}{b}\tilde{x}_i \qquad \text{(A3)}$$

for $i = 1$ to n, and $j = 1$ to m. The variables are cyclic so that $\tilde{y}_{i+n,j} = \tilde{y}_{i,j}$ and

$\tilde{y}_{i,j-m} = \tilde{y}_{i-1,j}$. We here set $n = 8$, $m = 4$, which gives a system dimension of

40, and forcing $\tilde{F} = 10$, for which the system is chaotic. See (Orrell and Smith,

2003).

The equations for the stochastic versions of the Lorenz '63 and Lorenz '96

systems are the same as above, but a stochastic term is added to each equation.

For example, Eq. A2 for the Lorenz '96 system becomes

$$\frac{dx_i}{dt} = x_{i-1}(x_{i+1} - x_{i-2}) - x_i + F + \Delta F\epsilon_i, \qquad \text{(A4)}$$

where ϵ_i is a random variable with standard deviation $\frac{1}{\sqrt{8}}$, so that the error over all

8 variables has magnitude ΔF. The value of ΔF is as specified.

The model for the Lorenz '63 system has the same equations, except that the

Reynold's number $R = 28.28$ has a one percent error. This introduces a dynamical

error in the equation for y, but not the other equations.

The model for the stochastic version of Lorenz '63 is the usual Lorenz '63 equations, so all error is due to the stochastic term in the system. Likewise for the stochastic version of Lorenz '96.

The model for the two-level system is the Lorenz '96 equations with forcing $F = 9.62$. This choice of forcing minimises the expected dynamical error. See (Orrell, 2003) for a detailed discussion of this model.

The Chua circuit is given by

$$
\begin{aligned}
\frac{dx}{dt} &= c_1(y - x - g(x)) \\
\frac{dy}{dt} &= c_2(x - y + z) \\
\frac{dz}{dt} &= -c_3 y,
\end{aligned}
\tag{A5}
$$

where

$$
g(x) = m_1 x + \frac{m_0 - m_1}{2}(\|x + 1\| - \|x - 1\|).
\tag{A6}
$$

Parameters are $c_1 = 15.6$, $c_2 = 1$, $c_3 = 25$, $m_0 = -8/7$, $m_1 = -5/7$. We define the model to be the above equations, while the true system to be shadowed has Gaussian stochastic dynamical terms $\Delta F = 1.0$, updated each $\Delta t = 0.01$.

The equations for the Vance-Gilpin model (with our choice of parameters) are:

$$
\begin{aligned}
\frac{dx_1}{dt} &= x_1(1 - 0.001x_1 - 0.001x_2 - 0.01x_3) \\
\frac{dx_2}{dt} &= x_2(1 - 0.0015x_1 - 0.001x_2 - 0.001x_3) \\
\frac{dx_3}{dt} &= x_3(-1 + cx_1 + 0.0005x_2).
\end{aligned}
\tag{A7}
$$

We use $c = 0.0025$, for which the model has a stable limit cycle attractor. The system has the same equations, but with dynamical noise added.

Finally, the weather model errors were obtained using the ECMWF operational model, relative to the ECMWF analysis, over a 15 day period in December 2000. See (Orrell et al., 2001; Orrell, 2002) for a detailed description. The model/system pairs are summarised in Table 1.

No.	System	Model	Dynamical Error
	Table 1: Model/System Pairs		
1	Lorenz '63 + stochastic terms	Lorenz '63	stoch. terms
2	Lorenz '96 + stochastic terms	Lorenz '96	stoch. terms
3	Lorenz '63 $R = 28$	Lorenz '63 $R = 28.28$	error in R
4	Two-level 40D $\tilde{F} = 10$	Lorenz '96 $F = 9.62$	parameterization
5	Chua circuit + stochastic terms	Chua circuit	stoch. terms
6	Vance-Gilpin + stochastic terms	Vance-Gilpin	stoch. terms
7	ECMWF analysis	Weather model	stoch. terms

Bibliography

Aguirre, L.A., and Billings, S.A., Validating identified nonlinear models with chaotic dynamics, *Int. J. Bifurcat. Chaos.*, **4**, 109-125, 1994.

Anosov, D., Geodesic flows and closed Riemannian manifolds with negative curvature, *Proc. Steklov Inst. Math.*, 1967.

Bowen, R., ω-limit sets for axiom A diffeomorphisms, *J. Diff. Eqns.*, **18**, 333-339, 1975.

Brown, R., Rulkov, N.F., and Tracy, E.R., Modeling and synchronizing chaotic systems from time-series data, *Phys. Rev. E*, **49**, 3784-3800, 1994.

Chu, P., Two kinds of predictability in the Lorenz system, *J. Atmos. Sci.*, **56**, 1427-1432, 1999.

Cohn, S., An introduction to estimation theory, *J. Meteorol. Soc. Japan*, **75**, 257-288, 1997.

Dennis, B., Desharnais, R.A., Cushing, J.M. and Constantino, R.F., Nonlinear demographic dynamics: mathematical models, statistical methods, and biological experiments. *Ecological Monographs*, **65**, 261-281, 1995.

Gillespie, D.T., A general method for numerically simulating the stochastic time evolution of coupled chemical reactions. *J. Comp. Phys.*, **22**, 403-434, 1976.

Gilmour, I., Nonlinear model evaluation: ι-shadowing, probabilistic predic-

tion and weather forecasting. *D. Phil. Thesis, Oxford University*, 1998.

Gilpin, M.E., Spiral chaos in a predator-prey model, *Am. Nat.*,**113**, 306-308, 1979.

Golub, G. and Loan, C., *Matrix Computations*, The John Hopkins University Press, 1989.

Gronnevik, R. and Evensen, G., Application of ensemble based techniques in fish-stock assessment. *Sarsia.*,**86**, 517-526, 2001.

Hansen, J., Accounting for model error in ensemble-based state estimation and forecasting, *Mon. Wea. Rev.*, **130**, 2373-2391, 2002.

Heald, J.P.M., and Stark, J., Estimations of noise levels for models of chaotic dynamical systems, *Phys. Rev. Lett.*, **84**, 2366-2369, 2000.

Judd, K. and Smith, L.A., Indistinguishable states 1: The perfect model scenario, *Physica D*, **151**, 125-141, 2001.

Keller, E.F., *Making Sense of Life*, Harvard University Press, 2002.

Klimko, L.A., and Nelson, P.I., On conditional least-squares estimates for stochastic processes. *Ann. Stat.*, **6**, 629-642, 1978.

Kostelich, E.J., and Yorke, J.A., Noise reduction: finding the simplest dynamical system consistent with the data. *Physica*, **41D**, 183, 1990.

Letellier, L., Le Sceller, L., Dutertre, P., Gouesbet, G., Fei, Z., and Hudson,

J.L., Topological characterization and global vector field reconstruction of an experimental electrochemical system. *J. Phys. Chem.*, **99**, 7016-7027, 1995.

Lorenz, E., Deterministic nonperiodic flow, *J. Atmos. Sci.*, **20**, 130-141, 1963.

Lorenz, E., Predictability - a problem partly solved, in *Predictability*, edited by T. Palmer, European Centre for Medium-Range Weather Forecasting, Shinfield Park, Reading UK, 1996.

Madan, R., *Chua's Circuit: A Paradigm for Chaos.* World Scientific, Singapore, 1993.

Matsumoto, T., Chua, L.O., and Komuro, M. *The double scroll.* IEEE Trans. Circuits Syst., **23**, 798-817, 1985.

Orrell, D., Modelling nonlinear dynamical systems: chaos, error and uncertainty. *D.Phil. thesis, Oxford University*, 2001.

Orrell, D., Smith, L., Barkmeijer, J., and Palmer, T., Model error in weather forecasting, *Nonlin. Proc. Geo.*, **8**, 357-371, 2001.

Orrell, D., Role of the metric in forecast error growth: how chaotic is the weather?, *Tellus*, **54A**, 350-362, 2002.

Orrell, D., and Smith, L.A., Visualizing bifurcations in high-dimensional systems: The spectral bifurcation diagram. *Int. J. Bifurcat. Chaos*, **13**, 3015-3027, 2003.

Orrell, D., Model error and predictability over different time scales in the Lorenz '96 systems, *J. Atmos. Sci.*, **60**, 2219-2228, 2003.

Orrell, D., Filtering chaos: A technique to estimate dynamical and observational noise in nonlinear systems, *Int. J. Bifurcat. Chaos*, in press, 2005.

Orrell, D., Ensemble forecasting in a system with model error, *J. Atmos. Sci.*, in press, 2005a.

Orrell, D., and Bolouri, H., Control of internal and external noise in genetic regulatory networks, *J. Theor. Biol.*, in press, 2004.

Ott, E., *Chaos in dynamical systems*, Cambridge University Press, 1993.

Ozaki, T., Jimenez, J.C., and Haggan-Ozaki, V., The role of the likelihood function in the estimation of chaos models, *J. Time Ser. Anal.*, **21**, 363-387, 2000.

Morohashi, M., Winn, A.E., Borisuk, M.T., Bolouri, H., Doyle, J., and Kitano, H., Robustness as a measure of plausibility in models of biochemical networks. *J. theor. Biol.*, **216**, 19-30, 2002.

Press, W.H., Flannery, B.P., Teukolsky, S.A., and Vetterling, W.T., *Numerical Recipes*, Cambridge University Press, 1986.

Robinson, A.R., McCarthy, J.J., and Rothschild, B.J. Interdisciplinary Ocean Science is Evolving and a Systems Approach is Essential, *Journal of Marine Systems*, **22**, 231-239, 1999.

Robinson, A.R. and Lermusiaux, P.F.J., Data Assimilation for Modeling and Predicting Coupled Physical-Biological Interactions in the Sea, Chapter 12 of *The Sea*, **12**, edited by Allan R. Robinson, James J. McCarthy and Brian J. Rothschild, John Wiley & Sons, Inc., New York, 2002.

Schreiber, T. and Kantz, H., Observing and predicting chaotic signals: Is 2% noise too much? *Predictability of complex dynamical systems*, edited by Y. Kravtsov and J. Kadtke, Springer, New York, 1996

Small, M., and Judd, K., Correlation dimension: A pivotal statistic for non-constrained realizations of composite hypotheses in surrogate data analysis, *Physica D*, **120**, 386-400, 1998.

Smith, L., Accountability in ensemble prediction. *Predictability*, edited by T. Palmer, European Centre for Medium-Range Weather Forecasting, Shinfield Park, Reading UK, 1996.

Smith, L.A., Ziehmann, C., and Fraedrich, K., Uncertainty Dynamics and Predictability in Chaotic Systems, *Q.J.R. Meteorol. Soc.*, **125**, 2855-2886, 1999.

Smith, L.A., Disentangling Uncertainty and Error: On the Predictability of Nonlinear Systems, in *Nonlinear Dynamics and Statistics*, 31-64, edited by A.I. Mees, Birkhauser, Boston, 2000.

Strang, G., 1986, *Introduction to applied mathematics*, Wellesley-Cambridge

Press.

Tong, H., 1990, *Nonlinear time series: a dynamical systems approach*, Oxford University Press.

Vance, R.R., Predation and resource partitioning in one-predator-two-prey model community, *Am. Nat.*,**112**, 797-813, 1978.

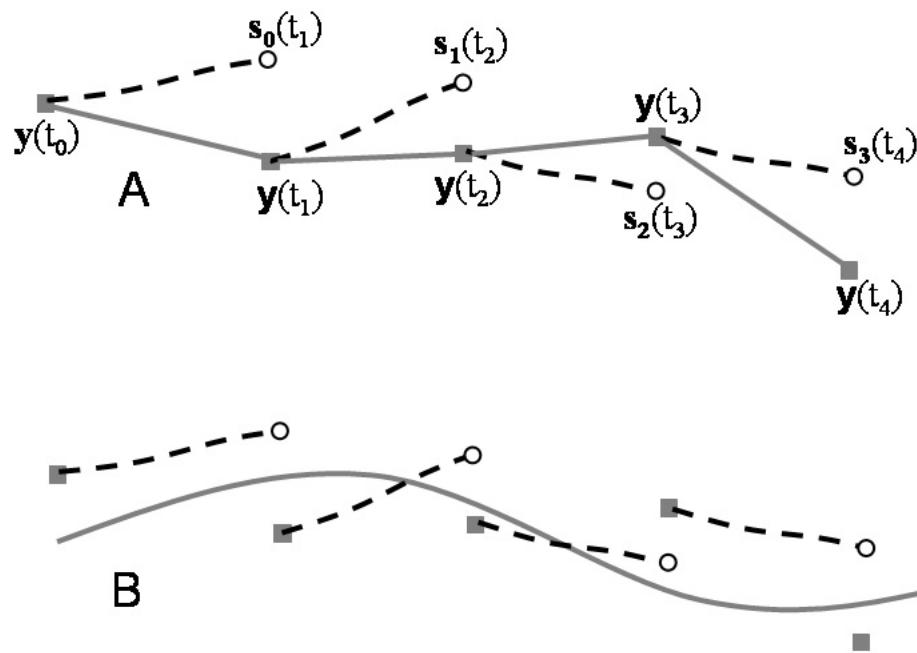Wiener, N., Differentiable space, *J. Math. and Phys.*,**2**, 131, 1923.

Figure 1: Schematic diagram showing observed system and short model forecasts. In panel A, the solid line represents a linear interpolation through the observed points $\mathbf{y}(t_j)$, while $\mathbf{s}_{j-1}(t_j)$ is the model forecast from the previous point. In panel B, the solid line represents a trajectory of the underlying system $\mathbf{x}(t)$. The points $\mathbf{y}(t_j)$ differ from this trajectory because of observational error. In either case, the observed forecast errors are the same.
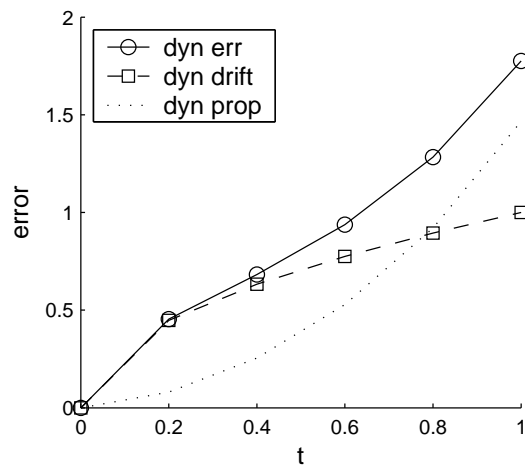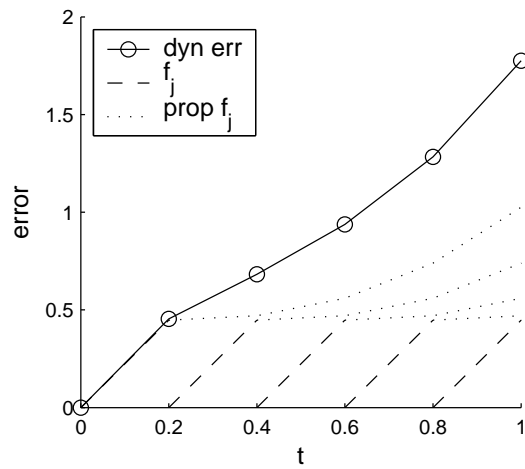
Figure 2: Schematic diagram of error components due to dynamical errors. The drift, shown in the lower panel, is calculated by summing the series of short forecast errors f_j in the upper panel. Each error here has the same magnitude, but is generally in a different direction. If the errors are assumed to be roughly orthogonal, then their sum grows in a square-root fashion. The effect of the propagated drift is to grow each short forecast error as shown by the dotted lines in the top panel. The result can be viewed as an additional term, shown in the lower panel by the dotted line, which adds orthogonally to the drift to create the total dynamical error (circle symbol).
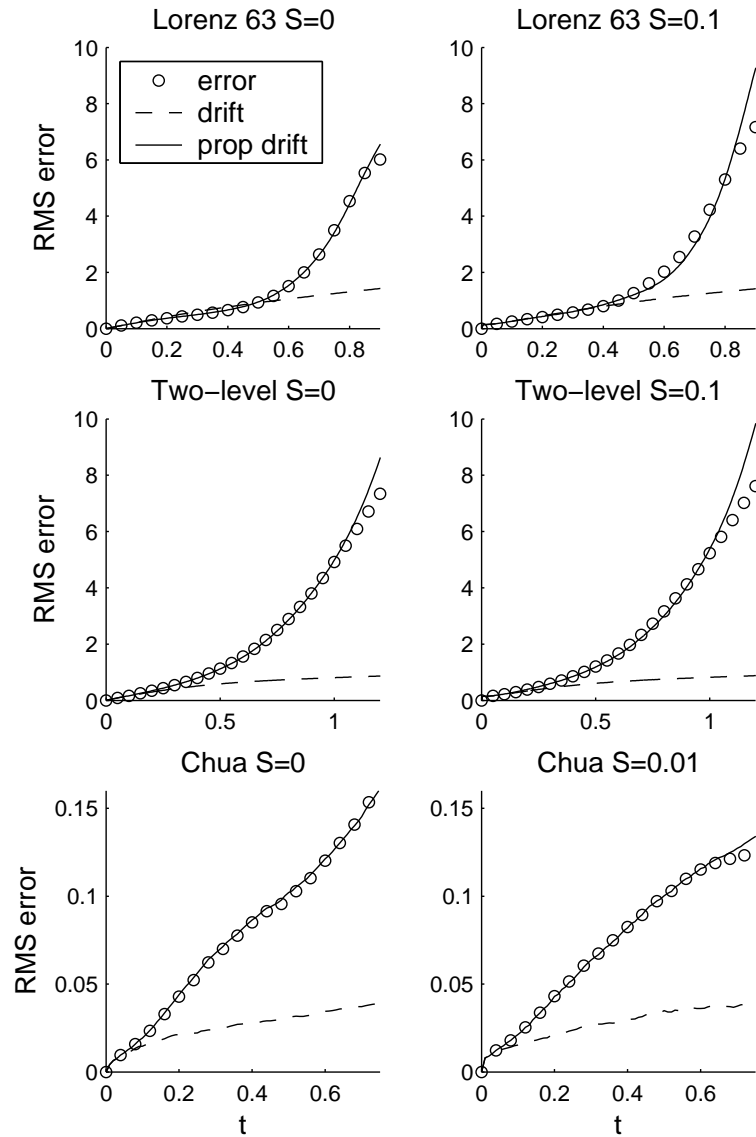
Figure 3: Error growth in three model/system pairs. Top panels show error in Lorenz '63 model due to a one percent error in the parameter R. Middle panels show errors in modeling the two level Lorenz '96 system with the constant model. Lower panels show the Chua circuit with stochastic dynamical errors of magnitude $\Delta F = 1$, updated each $\Delta t = 0.01$ time units. Left panels show case without observational error, right panels show case with Gaussian observation of standard deviation S. The propagated drift (solid line) is in each case a good fit to the forecast error. Model/system pairs used: 3, 4, 5 (see Table 1 in Appendix).
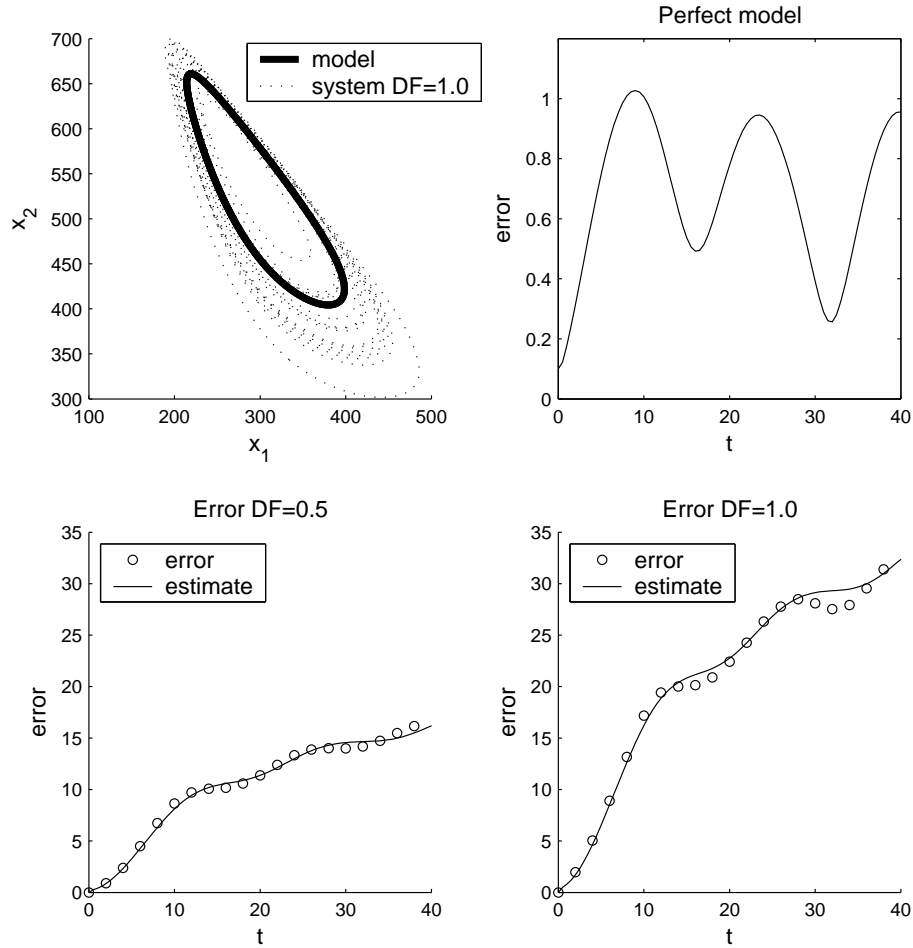
Figure 4: Error growth in the Vance-Gilpin system. For parameters as in the Appendix, the model describes a limit cycle, shown in the top left panel by the solid line. Also shown is a system orbit where dynamical terms with $\Delta F = 1.0$, $\Delta t = 0.5$ have been added to the system equations (see text). Top right panel shows error due to an initial perturbation of 0.1 in a perfect model experiment. The error grows over the first ten time units, then begins to oscillate. This curve defines the error propagation function $p(t)$ used to estimate the growth of forecast errors. The lower panels show error growth for $\Delta F = 0.5$ and $\Delta F = 1.0$, along with an estimate as described in text. Errors are RMS over 1000 runs. Model/system pair used: 6 (see Table 1 in Appendix).
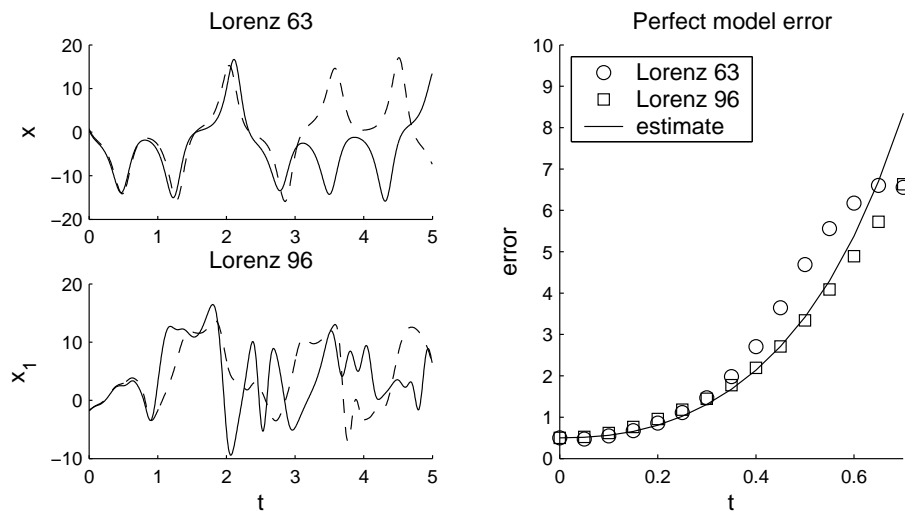
48

Figure 5: Left panels show typical time series for x in the Lorenz '63 system and x_1 in the 8D, $F = 13.2$ Lorenz '96 system. Dashed lines show orbits starting from a perturbation of magnitude 0.5. Right panels compare actual and estimated error growth due to an initial error of magnitude 0.5, for Lorenz '63 (circle symbol) and Lorenz '96 (square symbol). Solid line is given by Eq. 25, which is used to estimate the error propagation function $p(t)$. A time step of 0.005 is used for the Runge-Kutta integration scheme. The parameter a, which determines the exponential growth rate, was set to 4.1, which corresponds to a doubling time $t_d = 0.17$. Errors are RMS over 1000 runs.
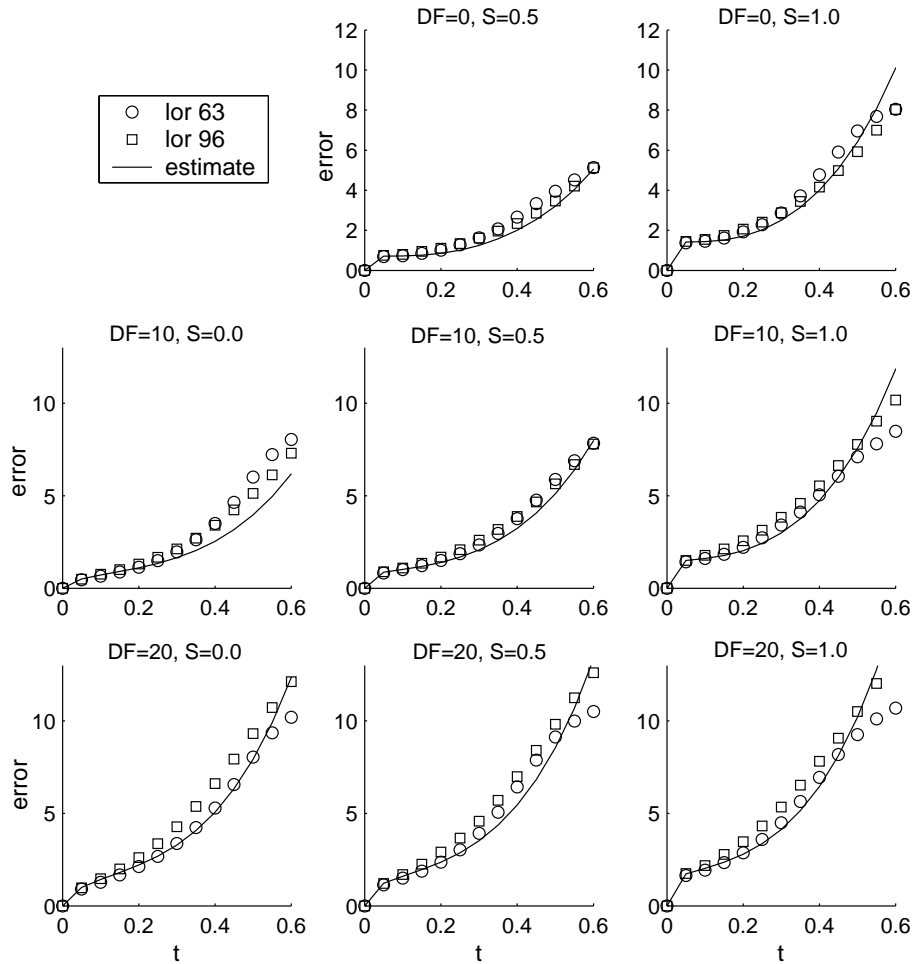
Figure 6: Comparison of actual and estimated error growth for Lorenz '63 (circle symbol) and 8D Lorenz '96 (square symbol). Dashed line is the estimate using Eq. 29. From the left to the right, observation error is $S = 0, 0.5$, and 1.0. From top to bottom, dynamical error is $\Delta F = 0$, 10, and 20. The timestep Δt, which mostly affects the relative strength of the dynamical error, is fixed at 0.05. A smaller time step of 0.005 is used for the Runge-Kutta integration scheme. The parameter a, which determines the exponential growth rate, was set to 4.1. Errors are measured relative to observations, so the error at time zero is zero. Model/system pairs used: 1 and 2.
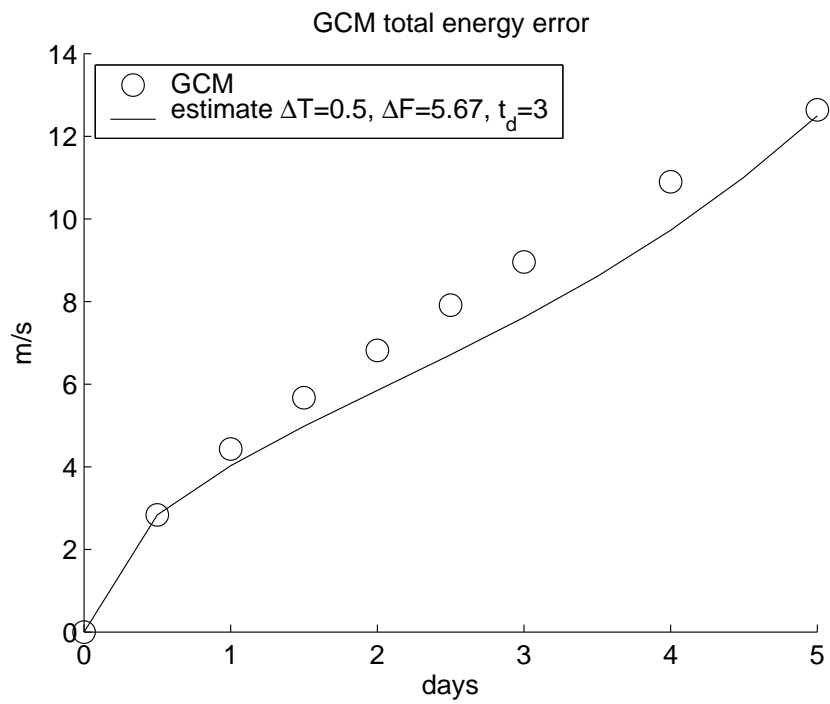
Figure 7: Comparison of total energy errors for the ECMWF operational model over a 15 day period in December 2000 (circle symbols), with an estimate obtained using Eq. 29 with timestep $\Delta t = 0.5$ days, model error $\Delta F = 5.67$, and doubling time $t_d = 3$.
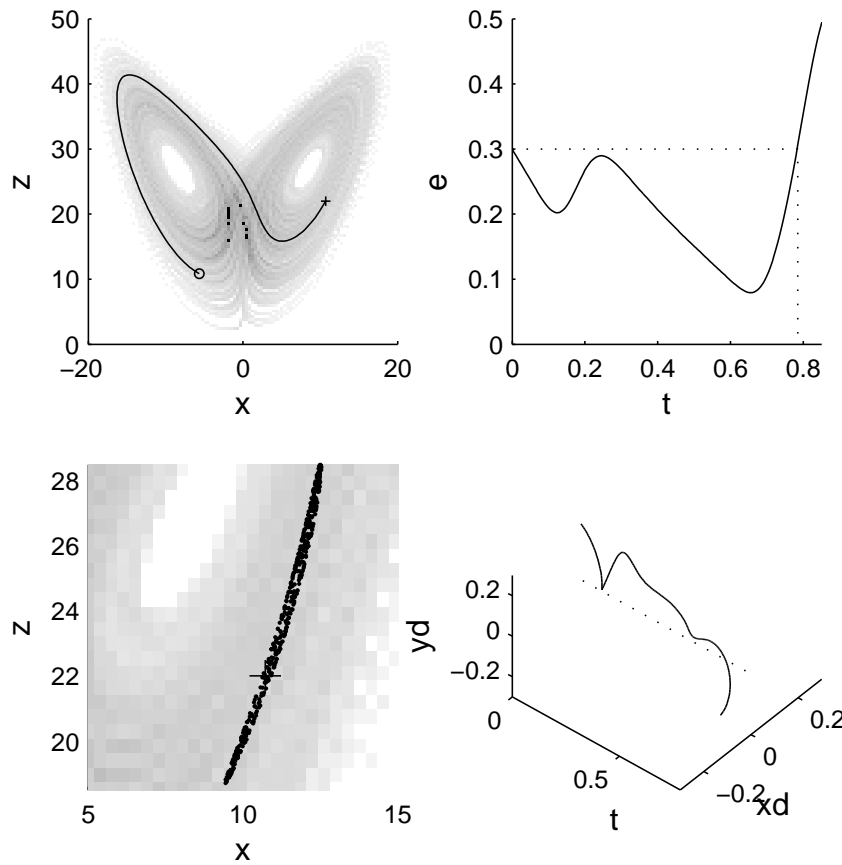
Figure 8: Views of a shadow orbit for the Lorenz '63 system. Model has a one percent error in parameter R. Shadow radius is $r = 0.3$. Clockwise from top left: portion of attractor shadowed, in $x - z$ plane, starting from point marked 'o' and ending at '+'; error of shadow orbit as a function of time; displacement of shadow orbit from true orbit, measured by projecting the error vector onto the plane tangent to the true orbit; zoomed view of radius 0.3 ensemble of points mapped forward under the model. The ball of points is mapped to a distorted ellipse under the nonlinear dynamics. Model/system pair used: 3.
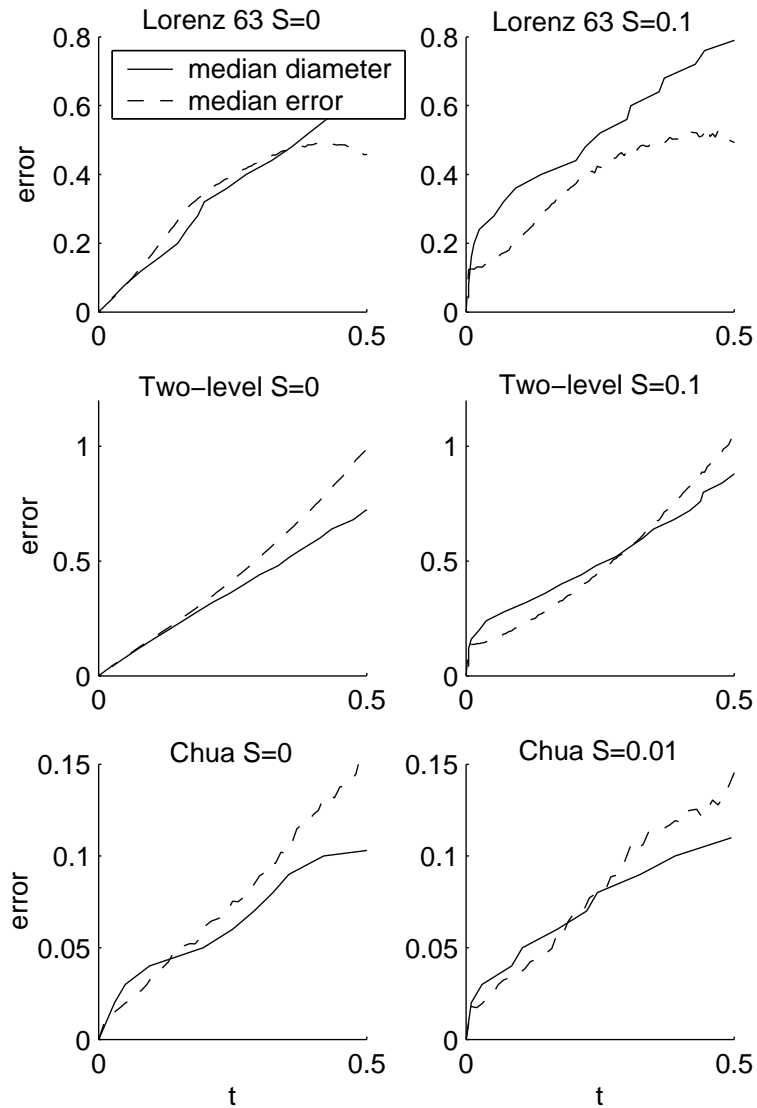
Figure 9: Plot comparing median forecast error as a function of time, with a reflected plot of median shadow time as a function of shadow diameter. Top panels are Lorenz '63 with a one percent error in the parameter R, middle panels are the two level Lorenz '96 system modeled with the constant model, lower panels are the Chua circuit with stochastic terms in the true system. Left panels show the case without observational error, in the right panels the system was observed with Gaussian errors of standard deviation $S = 0.1$. Model/system pairs used: 3, 4, 5.